

High-Temperature Annealing of AlGaN

Sylvia Hagedorn,* Taimoor Khan, Carsten Netzel, Carsten Hartmann, Sebastian Walde, and Markus Weyers

In the past few years, high-temperature annealing of AlN has become a proven method for providing AlN layers with low dislocation densities. Herein, the example of $\text{Al}_{0.77}\text{Ga}_{0.23}\text{N}$ is used to investigate whether annealing can also improve the material quality of the ternary alloy. A detailed analysis of the influence of annealing temperature on structural and optical material properties is presented. It is found that with increasing annealing temperature, the threading dislocation density can be lowered from an initial value of 6.0×10^9 down to $2.6 \times 10^9 \text{ cm}^{-2}$. Ga depletion at the AlGaN surface and Ga diffusion into the AlN buffer layer are observed. After annealing, the defect luminescence between 3 and 4 eV is increased, accompanied by an increase in the oxygen concentration by about two orders of magnitude. Furthermore, due to annealing optical absorption at 325 nm (3.8 eV) occurs, which increases with increasing annealing temperature. It is assumed that the reason for this decrease in ultraviolet (UV) transmittance is the increasing number of vacancies caused by the removal of group-III and N atoms from the AlGaN lattice during annealing.

1. Introduction

AlGaN grown on AlN/sapphire templates is a widely used approach to provide substrates for AlGaN-based light-emitting diodes (LEDs) with wavelength in the ultraviolet (UV) spectral range. Such LEDs can cover a wide range of applications, e.g., water purification, gas sensing, and medical treatments.^[1–4] To realize high output powers of the devices, the AlGaN heterostructures, in particular the active region, must be grown with a threading dislocation density (TDD) below 10^9 cm^{-2} .^[5] In the past few years, high-temperature annealing (HTA) at about

1700 °C has proven to be a viable method for decreasing the TDD of AlN buffer layers on sapphire substrates. Miyake et al. showed the usability of this technique for metalorganic vapor phase epitaxy (MOVPE)-grown AlN and sputtered AlN layers.^[6,7] For sputtered AlN, a TDD down to $2 \times 10^8 \text{ cm}^{-2}$ can be reached.^[8] For MOVPE-grown AlN, the lowest reported TDD after HTA is slightly higher at about $6 \times 10^8 \text{ cm}^{-2}$ and also meets the criterion of below 10^9 cm^{-2} .^[9] Stabilization against decomposition of the AlN surface during HTA is usually done by placing two AlN templates face to face.^[7] UVC LED heterostructures can be grown pseudomorphically on such low TDD AlN/sapphire templates without introducing new threading dislocations and therefore adopt the high material quality of the HTA template.^[10,11] AlGaN-based UVB LEDs with


Al mole fractions x of 0.6 or lower are more challenging. Due to the lattice mismatch between AlN and AlGaN, compressive strain during growth needs to be mastered. Otherwise, AlGaN relaxation can lead to surface roughening and formation of misfit dislocations during growth.^[12,13] Misfit dislocations can drastically increase the TDD by bending out of plane. Hence, providing low TDD $\text{Al}_x\text{Ga}_{1-x}\text{N}$ buffer layers instead of low TDD AlN buffers is desirable for UVA and UVB LEDs. As recently addressed in a review article about substrates for UV LEDs, our group investigates whether HTA can promote dislocation movement and annihilation in $\text{Al}_x\text{Ga}_{1-x}\text{N}$ layers, similar to the TDD reduction in MOVPE-grown AlN.^[14] To our knowledge, there are no other publications to date that investigate AlGaN annealing at temperatures of up to 1700 °C. Therefore, in this article, a detailed study of the influence of annealing temperature on the properties of $\text{Al}_{0.77}\text{Ga}_{0.23}\text{N}$ is presented.

2. Experimental Section

AlGaN samples were prepared by MOVPE in an AIX2400G3HT 11 × 2-in. planetary reactor. First, 630 nm-thick AlN was grown on c-plane-oriented sapphire with a nominal offcut of 0.2° toward m -direction as previously described by our group.^[9] In the following sections, this will be referred to as “AlN template.” $\text{Al}_x\text{Ga}_{1-x}\text{N}$ with Al mole fraction x of 0.77 was grown on the AlN template at a process temperature of 1150 °C and a total pressure of 50 mbar using H_2 as only carrier gas. As group-III precursors, 250 $\mu\text{mol min}^{-1}$ trimethylaluminum (TMAI) and 130 $\mu\text{mol min}^{-1}$ trimethylgallium (TMGa) were introduced into

Dr. S. Hagedorn, T. Khan, Dr. C. Netzel, S. Walde, Prof. M. Weyers
Ferdinand-Braun-Institut
Leibniz-Institut für Höchstfrequenztechnik
Gustav-Kirchhoff-Str. 4, Berlin 12489, Germany
E-mail: hagedorn@fbh-berlin.de

Dr. C. Hartmann
Application Science Department
Leibniz-Institut für Kristallzüchtung
Max-Born-Str. 2, Berlin 12489, Germany

 The ORCID identification number(s) for the author(s) of this article can be found under <https://doi.org/10.1002/pssa.202000473>.

© 2020 The Authors. Published by Wiley-VCH GmbH. This is an open access article under the terms of the Creative Commons Attribution License, which permits use, distribution and reproduction in any medium, provided the original work is properly cited.

The copyright line for this article was changed on 10 November 2020 after original online publication.

DOI: 10.1002/pssa.202000473

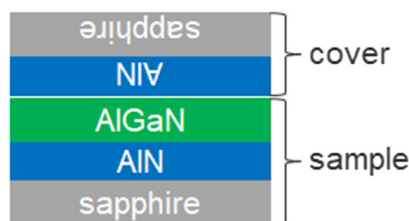


Figure 1. Sketch of the face-to-face arrangement used during HTA. AlGaN surfaces were covered with AlN templates.

the reactor, whereas ammonia served as group-V precursor. The input group-V-to-group-III ratio was kept constant at 30 during the whole deposition of 1.3 μm -thick $\text{Al}_{0.77}\text{Ga}_{0.23}\text{N}$. Afterward, AlGaN samples were placed in a carbon-free sinter oven and covered by an AlN template for HTA, as schematically shown in **Figure 1**. The samples were annealed in N_2 at 1000 mbar for 1 h at temperatures between 1605 and 1705 $^\circ\text{C}$. The temperature during HTA was measured with a type C thermocouple near the heated samples. Up to 1200 $^\circ\text{C}$, the heating rate was set to 10 K min^{-1} . For further temperature increase, a lower heating rate of 8 K min^{-1} up to 1600 $^\circ\text{C}$ followed by 4 K min^{-1} up to the targeted temperature was chosen to protect the oven equipment. To investigate the structural and morphological material properties before and after HTA, X-ray diffraction (XRD), scanning electron microscopy (SEM), atomic force microscopy (AFM), secondary-ion mass spectrometry (SIMS), and defect selective etching (DSE) were applied. Optical properties were investigated by SEM in combination with cathodoluminescence (CL) and by spectral transmission measurements. For measuring ω -rocking curves, high-resolution XRD measurements were carried out using a Malvern Panalytical X'Pert³ system with a four-fold 220 Ge monochromator and a $0.5 \times 5 \text{ mm}^2$ aperture on the source side and a triple axis configuration on the detector side. To depict XRD reciprocal space maps (RSMs), a PIXcel^{3D} array detector was used. Spatially resolved CL measurements were conducted at 80 K and 7 kV accelerating voltage in a Zeiss Ultra Plus field emission SEM with a Gatan MonoCL4 system. For transmission measurements, a setup was applied with

halogen and deuterium lamps on the source side and a fiber collecting the transmitted light on the detector side. Due to the limited acceptance angle of the fiber most of the stray light is not detected. An alkaline metal hydroxide melt was used for DSE of the AlGaN surface. A detailed description of the etching process will be published in previous studies.

3. Results and Discussion

$\text{Al}_{0.77}\text{Ga}_{0.23}\text{N}$ of 1.3 μm thickness was grown on a porous, 630 nm-thick AlN layer. **Figure 2a** shows an AFM image of the porous AlN template surface with nanoscale holes before AlGaN overgrowth. It should be mentioned that the porous AlN template was chosen to promote dislocation bending toward open sidewalls and relaxation of compressive strain in the AlGaN layer during the initial stages of growth. From the SEM cross-sectional image in **Figure 2b**, it can be concluded that after about 500 nm of $\text{Al}_{0.77}\text{Ga}_{0.23}\text{N}$ growth voids do not propagate further in growth direction. Hence, the AlGaN layer reaches its full coalescence at this point.

3.1. Structural and Morphological Properties of HTA AlGaN

AFM surface topograms show a hillock-like, cloudy surface morphology of the 1.3 μm -thick layer before HTA with a root-mean-square (RMS) roughness of 1.7 nm (**Figure 3a**). Due to annealing, the surface morphology changes toward a more step-like structure, which is already evident at 1605 $^\circ\text{C}$ through the faceting of the hillocks and an increase of the RMS value to 3.8 nm (**Figure 3b**). At high surface temperature, the adatoms can move on the surface and build up steps similar to the surface kinetics observed for MOVPE AlN grown at high temperatures.^[15] With increasing annealing temperature (**Figure 3c–e**), the free path length of the atoms on the surface increases. This results in a flattening of the surface hills and more extended terraces, which leads to a decrease in the RMS value to 1.9 nm up to an HTA temperature of 1680 $^\circ\text{C}$. Furthermore, some elongated ridges and small hills of about 4 nm height are formed, as exemplarily shown in **Figure 3e** by arrows. The elongated

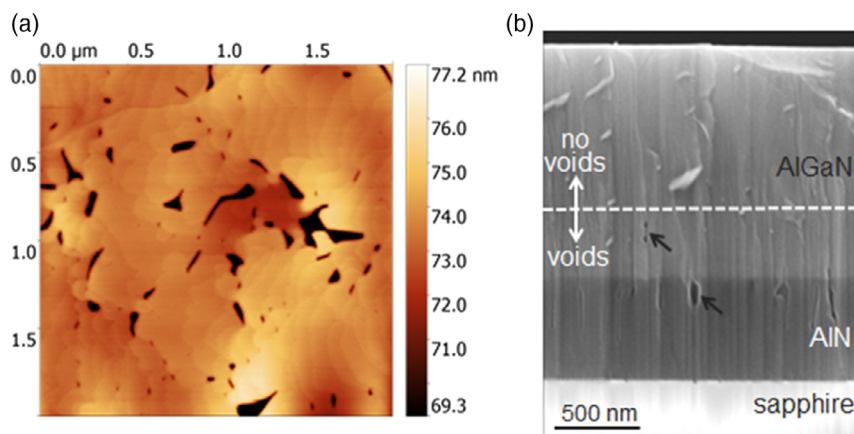


Figure 2. a) AFM surface topogram of 630 nm thick, porous AlN template layer. b) Cross-sectional SEM image of 1.3 μm $\text{Al}_{0.77}\text{Ga}_{0.23}\text{N}$ grown on such a template showing voids (exemplarily indicated by black arrows) and full coalescence after ≈ 500 nm of AlGaN growth (indicated by dashed line).

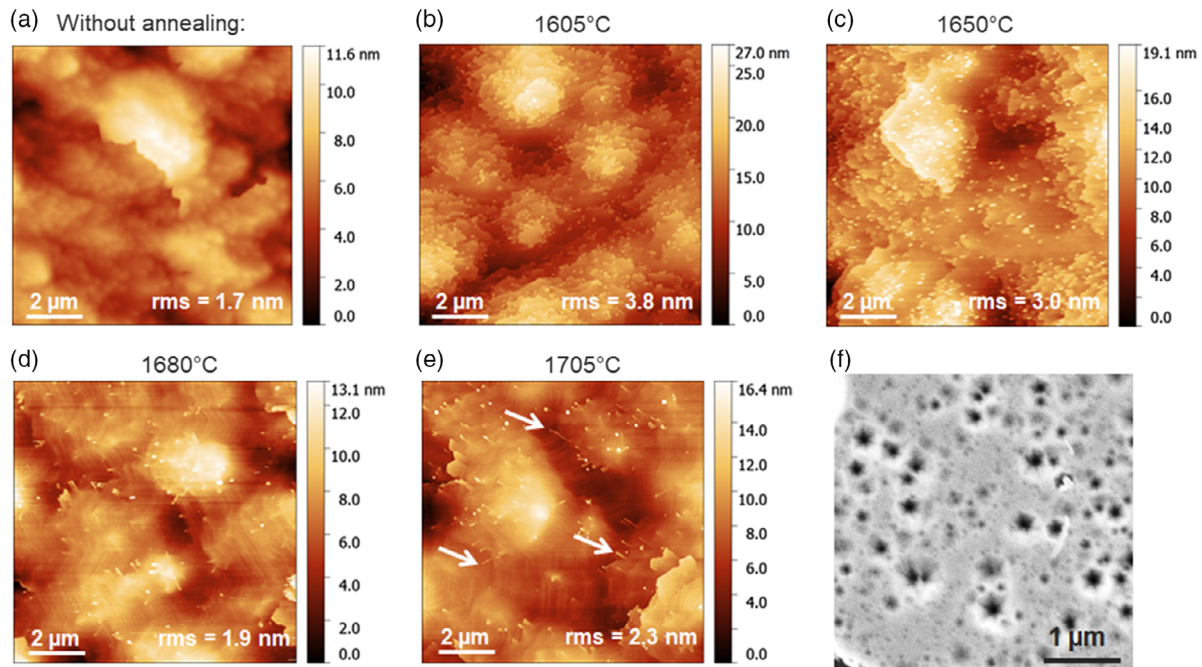


Figure 3. AFM surface topograms and corresponding RMS roughness values of $\text{Al}_{0.77}\text{Ga}_{0.23}\text{N}$ a) before and after 1 h of face-to-face annealing at b) 1605 °C, c) 1650 °C, d) 1680 °C, and e) 1705 °C. Arrows in (e) exemplarily mark positions of small ridges. f) SEM image showing the surface of the sample annealed at 1650 °C after defect selective etching.

stripes and small hills can be caused by pinned surface steps, which are locally prevented from moving. As expected from surface kinetics, for 1705 °C, the RMS value rises up to 2.3 nm due to formation of higher steps, ridges and small hills by step bunching.^[15] In terms of step height, the surfaces are all suitable for further overgrowth, e.g., with UV LED heterostructures.

XRD RSMs of the 0004 and 11–24 reflection (**Figure 4**) were measured to determine the Al mole fraction and strain state of the samples (**Table 1**). In the RSM of the sample before annealing, the two peaks of the 11–24 reflection of AlN and $\text{Al}_{0.77}\text{Ga}_{0.23}\text{N}$ are visible. In relation to the AlN template, the AlGaN layer is 66% relaxed. After annealing, the RSMs show counts between the AlN and AlGaN reflection (marked by dashed lines in **Figure 4b**). With increasing annealing temperature up to 1680 °C, the count rate between the AlN and AlGaN peak is increasing. This indicates formation of AlGaN with $x > 0.77$, i.e., an increasing loss in Ga from the AlGaN layer with increasing annealing temperature. To more closely investigate the origin of this effect, SIMS measurements were carried out to determine the intensity ratio of the GaCs^+ and AlCs^+ signals, which corresponds to the ratio of the Ga to Al signals, before and after annealing at 1680 °C (**Figure 5**).^[16] Comparison of both ratios clearly shows a less sharp AlGaN/AlN interface and also Ga depletion at the AlGaN surface due to annealing. From this, it can be concluded that HTA causes Ga diffusion into the AlN template layer and also Ga release from the AlGaN surface. Nevertheless, up to 1680 °C, the Al content of the main material and also the relaxation with respect to the underlying AlN is maintained (**Table 1**). Furthermore, compared with lower annealing temperatures, the 1680 °C sample shows a shift of the Q_z positions of the AlN and AlGaN reflection toward smaller values

in the RSM (**Figure 4**). This indicates an increased c lattice constant for AlN as well as for AlGaN. Assuming biaxial strain, the in-plane lattice constants of AlN and AlGaN are decreased leading to higher compressive strain in both layers after annealing. This increase in compressive strain is typically observed for HTA of AlN. It is attributed to rearrangement of AlN at high temperatures and the thermal mismatch between AlN and sapphire.^[7,17] For the highest temperature of 1705 °C, a significant Al mole fraction gradient is visible in the RSM by the shift and elongation of the AlGaN peak toward the AlN peak position along the dashed line in **Figure 4b**. The Al mole fraction increases to 0.80. The extension of the AlGaN peak in Q_x direction for the sample annealed at 1705 °C is smaller compared with lower annealing temperatures, which points to a less-pronounced relaxation variation or a less-pronounced relaxation gradient in the layer compared with the samples annealed at lower temperatures. From these findings, it can be concluded that at 1705 °C, the AlGaN lattice starts to rearrange under the release of Ga.

To investigate, the impact of HTA on the TDD in AlGaN and in the underlying AlN template full widths at half maximum of XRD ω -rocking curves (XRC-FWHM) of the 0002 and 10–12 reflection were measured (**Table 1**). To properly hit the AlGaN peak position in reciprocal space, the a and c lattice constants of AlGaN were estimated from the 0004 and 11–24 RSM shown in **Figure 4**. From these values, ψ and 2θ angles for skew-symmetrical XRD rocking-curve measurements were calculated. As **Table 1** shows, the XRC-FWHM of the 0002 reflection before annealing is already low and does not change significantly due to the annealing. This suggests a low tilt component of the material and regarding threading dislocations a low

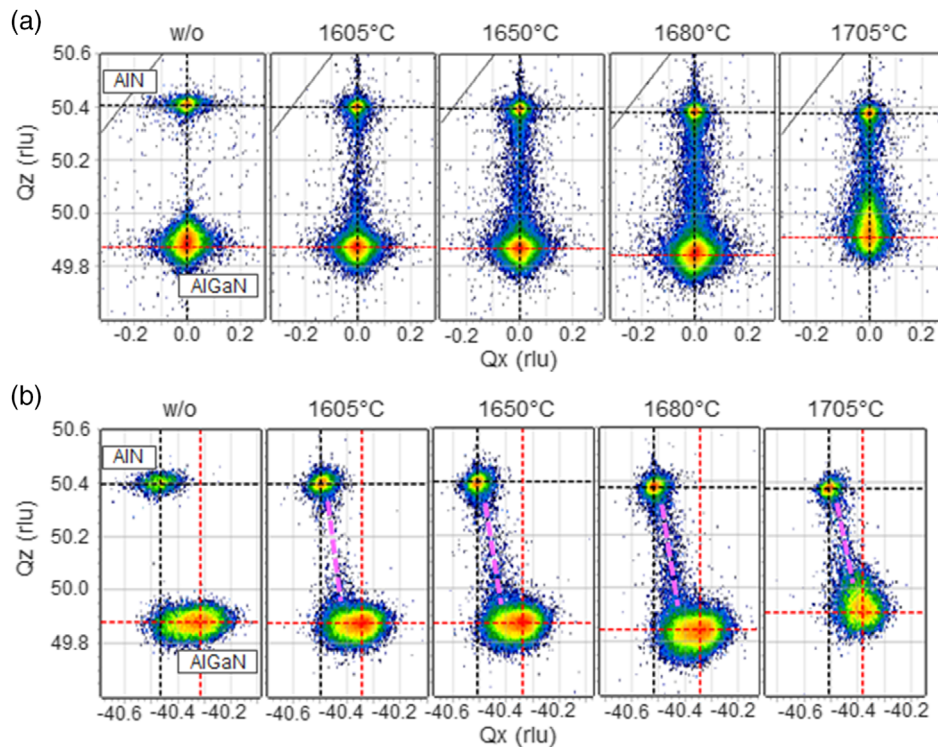


Figure 4. RSMs of 1.3 μm -thick $\text{Al}_{0.77}\text{Ga}_{0.23}\text{N}$ on AlN templates of the a) 0004 and b) 11–24 reflections without (w/o) and with annealing at temperatures ranging from 1605 to 1705 $^{\circ}\text{C}$. The positions of the AlN peak and the AlGaN peak are exemplarily labeled for the sample without annealing. For all annealed samples, an Al-mole fraction gradient can be observed by additional counts between the AlGaN and AlN lattice points (magenta dashed lines).

Table 1. Al-mole fraction x and in-plane relaxation of $\text{Al}_x\text{Ga}_{1-x}\text{N}$ toward the AlN base layer before and after annealing at temperatures between 1605 and 1705 $^{\circ}\text{C}$ calculated from the RSM in Figure 4. Corresponding XRC-FWHM for the 0002 and 10–12 reflections used for TDD estimation in Figure 6.

| $T_{\text{HTA}} [^{\circ}\text{C}]$ | x | Relaxation toward AlN [%] | XRC AlGaN 0002 [arcsec] | XRC AlGaN 10–12 [arcsec] | XRC AlN 0002 [arcsec] | XRC AlN 10–12 [arcsec] |
|-------------------------------------|------|---------------------------|-------------------------|--------------------------|-----------------------|------------------------|
| w/o HTA | 0.77 | 66 | 160 | 767 | 49 | 852 |
| 1605 | 0.77 | 69 | 128 | 537 | 68 | 514 |
| 1650 | 0.76 | 74 | 127 | 545 | 68 | 450 |
| 1680 | 0.76 | 72 | 151 | 582 | 77 | 385 |
| 1705 | 0.80 | 63 | 142 | 577 | 81 | 370 |

screw-type dislocation density in the AlN buffer and the AlGaN layer. The XRC-FWHM of the AlN 10–12 reflection decreases from 852 to 370 arcsec with increasing annealing temperature and therefore, despite of the AlGaN layer, behaves as usually observed for HTA of MOVPE-grown AlN.^[11,17] The trend of the 10–12 AlGaN XRC-FWHM is not as clear. For annealing temperatures up to 1650 $^{\circ}\text{C}$, it decreases from 767 to 545 arcsec, but increases to 580 arcsec for further increasing annealing temperature, indicating an increase in the twist component. This trend is reflected in the result of the TDD estimation from the XRC-FWHM accordingly (Figure 6), whereas the calculated TDD of the underlying AlN template decreases with increasing annealing temperature and reaches a value of $1.6 \times 10^9 \text{ cm}^{-2}$. For HTA of AlGaN up to 1650 $^{\circ}\text{C}$, the calculated TDD decreases from an initial value of 6.9×10^9 down to $3.5 \times 10^9 \text{ cm}^{-2}$. For annealing at higher temperatures, the estimated TDD increases

again to $3.9 \times 10^9 \text{ cm}^{-2}$. To distinguish whether the increase is caused by threading dislocation formation or due to other 10–12 XRC broadening mechanisms, e.g., the Al mole fraction gradient which was observed in the RSM (Figure 4), defect-selective etching was applied to the AlGaN sample surfaces. Figure 3f exemplarily shows the etched surface of AlGaN after annealing at 1650 $^{\circ}\text{C}$. Images of etched surfaces for all investigated HTA temperatures and before HTA can be found in Figure S1, Supporting Information. Big etch pits indicate screw-type dislocations, whereas smaller pits are formed at positions of edge-type and mixed dislocations.^[18] The etch pit density (EPD) decreases with increasing annealing temperature (Figure 6), which suggests a decrease in TDD from an initial value of 6.0×10^9 down to $2.6 \times 10^9 \text{ cm}^{-2}$ due to annealing at 1705 $^{\circ}\text{C}$. It is particularly striking that the increase in TDD calculated from XRC-FWHM for the samples annealed at

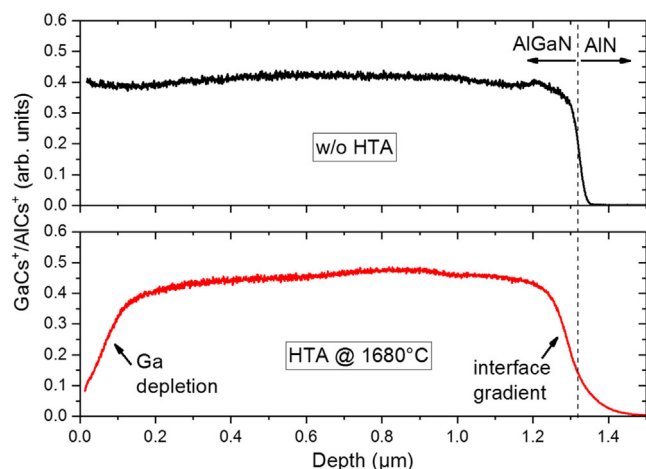


Figure 5. Depth-dependent $\text{GaCs}^+/\text{AlCs}^+$ signal ratio from SIMS measurements for 1.3 μm AlGaN before and after HTA at 1680 $^\circ\text{C}$.

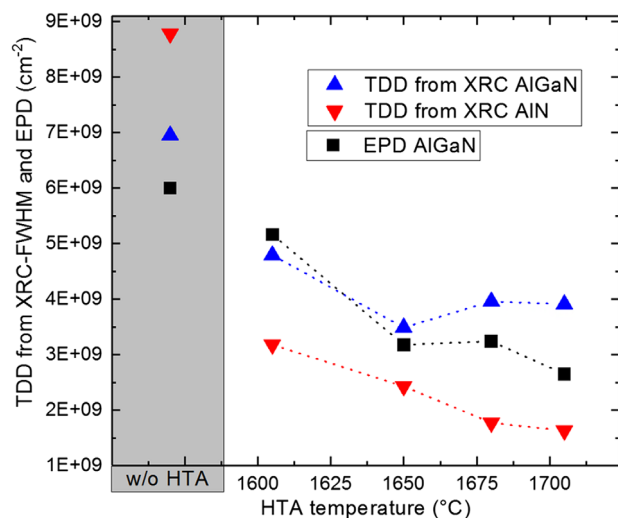


Figure 6. EPD of $\text{Al}_{0.77}\text{Ga}_{0.23}\text{N}$ and TDD estimated from XRC-FWHM of the 0002 and 10–12 reflections for AlN and $\text{Al}_{0.77}\text{Ga}_{0.23}\text{N}$ (Table 1) plotted against the annealing temperature.

temperatures above 1650 $^\circ\text{C}$ is not confirmed by the EPD. It can therefore be assumed that by annealing AlGaN at high temperatures further broadening mechanisms of the XRC lead to an overestimation of the calculated TDD. Furthermore, the EPD for the 1650 and 1680 $^\circ\text{C}$ samples are almost identical. To answer the question whether there is a kind of TDD “saturation effect” and TDD can only be further decreased with decreasing Ga mole fraction would require composition-dependent studies which go beyond the scope of this study.

3.2. Optical Properties of HTA AlGaN

With increasing annealing temperature, an increasing brown discoloration of the previously transparent AlGaN samples is observed. This change in color indicates the absorption of light

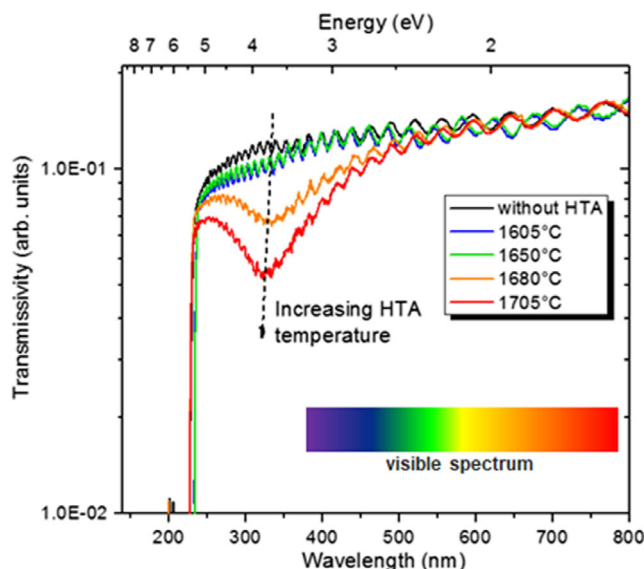


Figure 7. Transmittance through $\text{Al}_{0.77}\text{Ga}_{0.23}\text{N}$ before and after annealing at different temperatures. With increasing HTA temperature, absorption around 325 nm increases (arrow).

in the visible spectral range with wavelength shorter than green. To investigate the absorption more in depth, transmission measurements were conducted (Figure 7). It should be noted that the measurement setup has a relatively low acceptance angle, which causes stray light losses at the unpolished sapphire backside of the samples. Optical absorption around 325 nm (3.8 eV) becomes more and more distinct with increasing annealing temperature. The absorption band around 325 nm expands into the visible range causing the brown discoloration. For AlN, Bickermann et al. tentatively assigned optical absorption at 3.9 eV to a transition from negatively charged Al vacancies to the conduction band or to a shallow donor.^[19] Yan et al. concluded that absorption in AlN around 4.0 eV is caused by complexes of an Al vacancy and oxygen impurities.^[20] The unchanged position of the AlGaN absorption edge after HTA (Figure 7) confirms that the Al-mole fraction in the main part of the AlGaN layer remains almost unchanged, which was already derived from the XRD RSM in Figure 4. However, a blue shift of the absorption peak can be detected with increasing annealing temperature. A possible explanation can be a higher density of donor and acceptor like defect states involved in the associated transition as well as a higher bandgap by Ga loss in parts of the AlGaN layer.^[21]

CL spectra were taken along the cross-sections of the non-annealed $\text{Al}_{0.77}\text{Ga}_{0.23}\text{N}$ sample, and the sample annealed at 1680 $^\circ\text{C}$ to investigate the optical properties with depth resolution (Figure 8). Before annealing, the near band edge (NBE) luminescence of the 1.3 μm -thick AlGaN layer slightly shifts toward lower energy with increasing AlGaN layer thickness after ≈ 500 nm of growth (Figure 8a). As Figure 5 shows, this cannot be explained by a higher Ga mole fraction. However, as the AlGaN layer is partially relaxed (Table 1), the redshift is most likely caused by an increasing degree of relaxation. Due to HTA, no significant change in the NBE luminescence position, but a change in

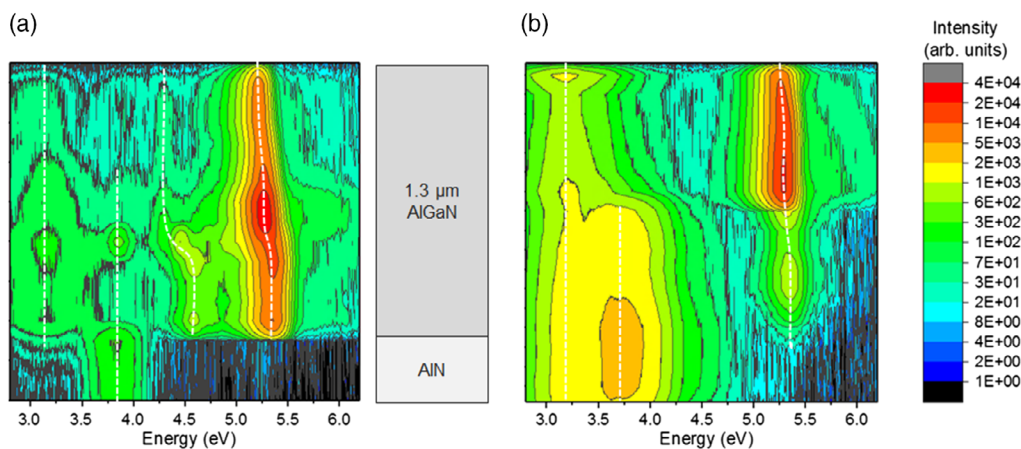


Figure 8. CL measurements taken at 80 K and 7 kV along the cross section of 1.3 μm $\text{Al}_{0.77}\text{Ga}_{0.23}\text{N}/\text{AlN}$ a) before and b) after annealing at 1680 $^{\circ}\text{C}$.

the intensity can be observed (Figure 8b). After HTA, the AlGaN close to the AlN buffer shows a decreased NBE luminescence intensity, most probably caused by the simultaneous strong increase in defect luminescence. The upper part of the AlGaN layer shows an increased NBE intensity, which indicates that the detected reduced TDD leads to more efficient light generation. However, this would still have to be confirmed by temperature-dependent intensity measurements up to room temperature. Note that the CL measurement of the annealed sample, despite of the near-surface Ga depletion observed in SIMS measurements (Figure 5), does not show a significant blue shift. The higher bandgap and surface fields seem to suppress charge carrier recombination in the Ga-depleted layer.

Before annealing, defect luminescence was observed at 3.2, 3.8, and around 4.5 eV (Figure 8a). In general, the underlying AlN template and the AlGaN layer show increased defect luminescence intensity between 3.0 and 4.0 eV after annealing while the defect luminescence around 4.5 eV is not visible anymore (Figure 8b). As the related optical transitions are assigned to point defects, SIMS measurements were carried out to quantitatively determine the concentration of typical impurities like O, Si, and C (Figure 9). Due to HTA, the Si concentration in the upper 500 nm of AlGaN increases from

4×10^{16} to $2 \times 10^{18} \text{ cm}^{-3}$, but remains essentially unchanged in the remaining sample (Figure 9a). The increased Si concentration may also contribute to the increased CL intensity of the near-surface NBE luminescence after annealing. As the whole oven setup is free of Si, Si most probably originates from exposure of the AlGaN surface to air before annealing. Si accumulation due to exposure to the ambient air is a known problem for compound semiconductors.^[22,23] Due to the high temperature, the Si then diffuses from the surface into the bulk. The C concentration in the AlGaN layer stays constant at $2 \times 10^{18} \text{ cm}^{-3}$ and is not changed by HTA (Figure 9b). Most striking is the strong increase in oxygen concentration in AlN and AlGaN by two orders of magnitude from 10^{17} to 10^{19} cm^{-3} for AlGaN and from 10^{19} to 10^{20} cm^{-3} for AlN (Figure 9c). O sources can be the sapphire substrate, O attached to the AlGaN surface or the aluminum oxide parts of the oven setup. Anyway, the increased O concentration in conjunction with Ga removal from the lattice due to HTA is a good candidate to explain the increase in defect luminescence intensity (Figure 8b). In literature, for AlN and $\text{Al}_{0.75}\text{Ga}_{0.25}\text{N}$, the violet luminescence band around 3.4 eV (including 3.2 and 3.8 eV) is associated to charged Al vacancies ($\text{V}_{\text{Al}}^{2-/3-}$) and charged Al vacancy – oxygen complexes ($\text{V}_{\text{Al}}\text{-O}_{\text{N}}^{-/2-}$).^[20,24] The

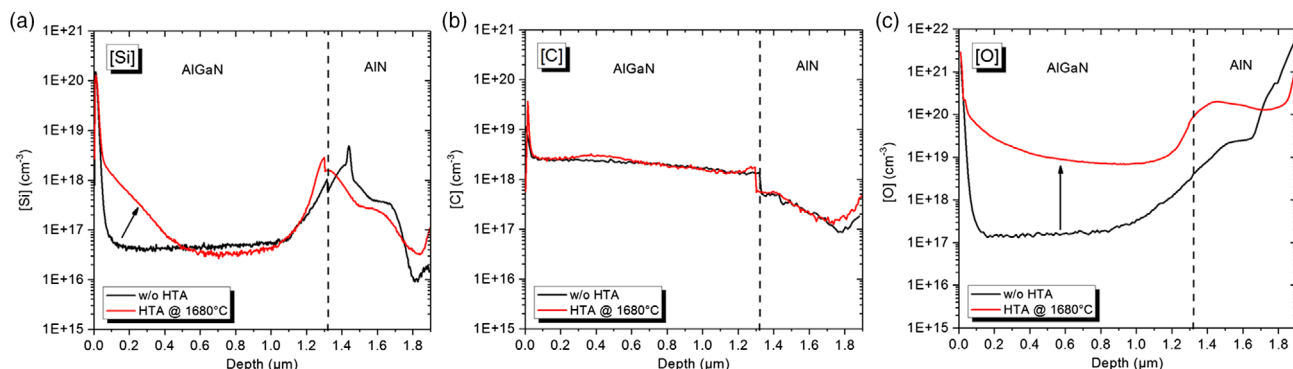


Figure 9. Quantitative SIMS analysis of a) [Si], b) [C], and c) [O] impurity concentration in AlGaN and AlN before and after annealing at 1680 $^{\circ}\text{C}$. Significant changes in the profiles are indicated by arrows. Abrupt changes in concentration at the AlGaN–AlN interface are due to the fact that different SIMS standards were used for AlGaN and AlN.

luminescence around 4.5 eV, which we observe only in AlGa_N is also associated to a transition to a negatively charged vacancy complex.^[19,25] Hence, HTA is introducing charged group-III vacancies and complexes with oxygen into the AlN and AlGa_N layer. In the upper AlGa_N part, the defect luminescence at 3.2 eV is dominant. Bickermann et al. have correlated defect luminescence at 3.3 eV with optical absorption at 3.9 eV for AlN.^[19] Yan et al. observed a correlation between emission at 3.2–3.5 eV and absorption around 4 eV.^[20] It is therefore very likely that the defect luminescence at 3.2 eV is related to the absorption at 325 nm in AlGa_N after annealing (Figure 7). It is assumed that the surface layer, which is particularly affected by Ga desorption, has considerably more group-III vacancies than the layer below and could therefore contribute more to absorption. Unfortunately, absorption at 325 nm is disadvantageous for the targeted application as substrate for UVB LEDs, because the EQE of the devices, which are usually designed as bottom emitters, is reduced. Furthermore, it should be noted that HTA could also lead to absorption by formation of group-III and N vacancies, which are suspected of being able to cluster and form nonradiative recombination centers.^[26] The aim of further process optimization must in any case be to avoid UV absorption and hence to avoid the formation of intrinsic defects during AlGa_N annealing.

4. Conclusion

We investigated the influence of annealing temperature on structural and optical material properties of Al_{0.77}Ga_{0.23}N. It was found that with increasing annealing temperature up to 1705 °C, the TDD can be lowered from an initial value of 6.0×10^9 down to 2.6×10^9 cm⁻². Ga depletion at the AlGa_N surface and Ga diffusion into the AlN buffer layer is observed for all annealing temperatures between 1605 and 1705 °C. In addition to that, up to 1680 °C, the Al_{0.77}Ga_{0.23}N is largely temperature-stable, whereas at 1705 °C, the Ga mole fraction decreases from 0.23 to 0.20, indicating partial decomposition by loss of Ga. After annealing at 1680 °C, the defect luminescence between 3 and 4 eV is increased, accompanied by an increase in the oxygen concentration by about two orders of magnitude. The values for other impurity concentrations such as [Si] and [C] remain largely unchanged at 4×10^{16} and 2×10^{18} cm⁻³, respectively. Furthermore, due to annealing optical absorption at 325 nm (3.8 eV) occurs, which increases with increasing annealing temperature. It is assumed that the formation of vacancies plays a vital role in the decreased UV transmittance of HTA AlGa_N.

Supporting Information

Supporting Information is available from the Wiley Online Library or from the author.

Acknowledgements

This work was partially funded by the German Federal Ministry of Education and Research (BMBF) within the Advanced UV for Life project consortium and by the German Research Foundation (DFG) within the

Collaborative Research Center “Semiconductor Nanophotonics” (CRC 787). Furthermore, the authors thank Torsten Petzke from FBH for technical assistance with the MOVPE machine. Open access funding enabled and organized by Projekt DEAL.

Conflict of Interest

The authors declare no conflict of interest.

Keywords

AlGa_N, high-temperature annealing, metalorganic vapor phase epitaxy, substrate, ultraviolet light-emitting diodes

Received: July 22, 2020

Revised: September 7, 2020

Published online: October 7, 2020

- [1] W. L. Morison, T. B. Fitzpatrick, *Phototherapy and Photochemotherapy of Skin Disease*, 2nd ed., Raven Press, New York **1991**.
- [2] M. Kneissl, J. Rass, in *III-Nitride Ultraviolet Emitters*, Springer Series in Materials Science, Springer, Berlin/New York **2016**.
- [3] M. Würtele, T. Kolbe, M. Lipsz, A. Külberg, M. Weyers, M. Kneissl, M. Jekel, *Water Res.* **2011**, *45*, 1481.
- [4] H. Hirayama, T. Yatabe, N. Noguchi, N. Kamata, *Electron. Commun. Jpn.* **2010**, *93*, 24.
- [5] M. Kneissl, T. Kolbe, C. Chua, V. Kueller, N. Lobo, J. Stellmach, A. Knauer, H. Rodriguez, S. Einfeldt, Z. Yang, N. M. Johnson, M. Weyers, *Semicond. Sci. Technol.* **2011**, *26*, 014036.
- [6] H. Miyake, G. Nishino, S. Suzuki, K. Hiramatsu, H. Fukuyama, J. Kaur, N. Kuwano, *Appl. Phys. Express* **2016**, *9*, 025501.
- [7] H. Miyake, C.-H. Lin, K. Tokoro, K. Hiramatsu, *J. Cryst. Growth* **2016**, *456*, 155.
- [8] K. Uesugi, Y. Hayashi, K. Shojiki, H. Miyake, *Appl. Phys. Express* **2019**, *12*, 065501.
- [9] S. Walde, S. Hagedorn, M. Weyers, *Jpn. J. Appl. Phys.* **2019**, *58*(SC), SC1002.
- [10] N. Susilo, S. Hagedorn, D. Jaeger, H. Miyake, U. Zeimer, C. Reich, B. Neuschulz, L. Sulmoni, M. Guttman, F. Mehnke, C. Kuhn, T. Wernicke, M. Weyers, M. Kneissl, *Appl. Phys. Lett.* **2018**, *112*, 041110.
- [11] M. X. Wang, F. J. Xu, N. Xie, Y. H. Sun, B. Y. Liu, Z. X. Qin, X. Q. Wang, B. Shen, *Cryst. Eng. Commun.* **2018**, *20*, 6613.
- [12] Y. Kawase, S. Ikeda, Y. Sakuragi, S. Yasue, S. Iwayama, M. Iwaya, T. Takeuchi, S. Kamiyama, I. Akasaki, H. Miyake, *Jpn. J. Appl. Phys.* **2019**, *58*, SC1052.
- [13] Z. Wu, K. Nonaka, Y. Kawai, T. Asai, F. A. Ponce, Ch Chen, M. Iwaya, S. Kamiyama, H. Amano, I. Akasaki, *Appl. Phys. Express* **2010**, *3*, 11003.
- [14] S. Hagedorn, S. Walde, A. Knauer, N. Susilo, D. Pacak, L. Cancellara, C. Netzel, A. Mogilatenko, C. Hartmann, T. Wernicke, M. Kneissl, M. Weyers, *Phys. Status Solidi A* **2020**, 1901022.
- [15] I. Bryan, Z. Bryan, S. Mita, A. Rice, J. Tweedie, R. Collazo, Z. Sitar, *J. Cryst. Growth* **2016**, *438*, 81.
- [16] C. J. Gu, F. A. Stevie, C. J. Hitzman, Y. N. Saripalli, M. Johnson, D. P. Griffis, *Appl. Surf. Sci.* **2006**, *252*, 7228.
- [17] M. X. Wang, F. J. Xu, N. Xie, Y. H. Sun, B. Y. Liu, W. K. Ge, X. N. Kang, Z. X. Qin, X. L. Yang, X. Q. Wang, B. Shen, *Appl. Phys. Lett.* **2019**, *114*, 112105.

- [18] K. Moszak, W. Olszewski, D. Pucicki, J. Serafinczuk, K. Opotczynska, M. Rudzinski, R. Kudrawiec, D. Hommel, *J. Appl. Phys.* **2019**, 126, 165304.
- [19] M. Bickermann, B. M. Epelbaum, O. Filip, P. Heimann, S. Nagata, A. Winnacker, *Phys. Status Solidi B* **2009**, 246, 1181.
- [20] Q. Yan, A. Janotti, M. Scheffler, C. Van de Walle, *Appl. Phys. Lett.* **2014**, 105, 111104.
- [21] E. M. Kazaryan, A. A. Kostanyan, H. A. Sarkisyan, *J. Phys.: Condens. Matter* **2007**, 19, 046212.
- [22] M. Monavarian, G. Pickrell, A. A. Aragon, I. Stricklin, M. H. Crawford, A. A. Allerman, K. C. Celio, F. Léonard, A. A. Talin, A. M. Armstrong, D. Feezell, *IEEE Electron Device Lett.* **2019**, 40, 387.
- [23] A. Armstrong, D. Feezell, A. A. Allerman, G. Pickrell, M. Monavarian, I. Stricklin, M. H. Crawford, K. C. Celio, F. Leonard, A. A. Talin, Sandia Nat. Lab., Albuquerque, NM, USA, Tech. Rep. SAND2018-2511C, <https://www.osti.gov/biblio/1427304> (accessed: June 2020).
- [24] T. Koppe, H. Hofsäss, U. Vetter, *J. Lumin.* **2016**, 178, 267.
- [25] N. Nepal, M. L. Nakarmi, J. Y. Lin, H. X. Jiang, *Appl. Phys. Lett.* **2006**, 89, 092107.
- [26] S. F. Chichibu, A. Uedono, K. Kojima, H. Ikeda, K. Fujito, S. Takashima, M. Edo, K. Ueno, S. Ishibashi, *J. Appl. Phys.* **2018**, 123, 161413.